

Disordered Tm:Ca₉La(VO₄)₇: a novel crystal with potential for broadband tunable lasing

Z. ZHANG,^{1,2} P. LOIKO,³ H. WU,¹ X. MATEOS,^{4,5,10,*} J. M. SERRES,⁴ H. F. LIN,¹ W. D. CHEN,^{1,5,8} G. ZHANG,¹ L. Z. ZHANG,^{1,7} F. DÍAZ,⁴ M. AGUILÓ,⁴ V. PETROV,⁵ U. GRIEBNER,⁵ Y. C. WANG,⁵ E. VILEJSHIKOVA,⁶ K. YUMASHEV,⁶ AND Z. B. LIN^{1,7,9}

¹Key Laboratory of Optoelectronic Materials Chemistry and Physics, Fujian Institute of Research on the Structure of Matter, Chinese Academy of Sciences, 350002 Fuzhou, China

²Graduate School of Fujian Normal University, 350117 Fuzhou, China

³ITMO University, 49 Kronverkskiy pr., St. Petersburg 197101, Russia

⁴Física i Cristal·lografia de Materials i Nanomaterials (FiCMA-FiCNA), Universitat Rovira i Virgili (URV), Campus Sescelades, c/ Marcel·lí Domingo, s/n., E-43007 Tarragona, Spain

⁵Max Born Institute for Nonlinear Optics and Short Pulse Spectroscopy, Max-Born-Str. 2a, D-12489 Berlin, Germany

⁶Center for Optical Materials and Technologies (COMT), Belarusian National Technical University, 65/17 Nezavisimosti Ave., 220013 Minsk, Belarus

⁷State Key Laboratory of Structural Chemistry, 350002 Fuzhou, China

⁸chenweidong@fjirsm.ac.cn

⁹lzb@fjirsm.ac.cn

¹⁰mateos@mbi-berlin.de

*xavier.mateos@urv.cat

Abstract: We report on the crystal growth, structural and spectroscopic investigation of a novel trigonal calcium vanadate crystal, Tm³⁺:Ca₉La(VO₄)₇. Polarized absorption, stimulated-emission and gain cross-section spectra are determined for this material. The maximum σ_{SE} corresponding to the ³F₄ → ³H₆ transition amounts to 1.28×10^{-20} cm² at 1854 nm for σ -polarization. The measured lifetime of the Tm³⁺ ions in the ³F₄ state is 1.19 ms. The Judd-Ofelt analysis performed yielded intensity parameters of $\Omega_2 = 4.682$, $\Omega_4 = 0.659$ and $\Omega_6 = 0.475$ [10^{-20} cm²]. The polarized Raman spectra indicate a strong and broad band centered at 867 cm⁻¹. Owing to the disordered nature of Ca₉La(VO₄)₇, the Tm³⁺ ions exhibit a broad and smooth gain profile at ~2 μ m. The spectroscopic properties of Tm³⁺:Ca₉La(VO₄)₇ are very promising for broadly tunable and ultrashort pulse lasers near 2 μ m.

© 2017 Optical Society of America

OCIS codes: (140.3380) Laser materials, (300.0300) Spectroscopy; (140.3480) Lasers, diode-pumped.

References and links

1. A. A. Kaminskii, "Laser crystals and ceramics: recent advances," *Laser Photonics Rev.* **1**(2), 93–177 (2007).
2. J. Petit, B. Viana, P. Goldner, D. Vivien, P. Louiseau, and B. Ferrand, "Laser oscillation with low quantum defect in Yb:GdVO₄, a crystal with high thermal conductivity," *Opt. Lett.* **29**(8), 833–835 (2004).
3. J. Liu, V. Petrov, H. Zhang, J. Wang, and M. Jiang, "High-power laser performance of *a*-cut and *c*-cut Yb:LuVO₄ crystals," *Opt. Lett.* **31**(22), 3294–3296 (2006).
4. Yu. D. Zavartsev, P. A. Studenikin, V. A. Mikhailov, A. I. Zagumennyi, G. Huber, E. Heumann, V. G. Ostroumov, and I. A. Shcherbakov, "Tm³⁺:GdVO₄ – a new efficient medium for diode-pumped 2- μ m lasers," *Quantum Electron.* **27**(1), 13–14 (1997).
5. X. Mateos, J. Liu, H. Zhang, J. Wang, M. Jiang, U. Griebner, and V. Petrov, "Continuous-wave and tunable laser operation of Tm:LuVO₄ near 1.9 μ m under Ti:sapphire and diode laser pumping," *Phys. Status Solidi* **203**(4), R19–R21 (2006).
6. S. Rivier, X. Mateos, J. Liu, V. Petrov, U. Griebner, M. Zorn, M. Weyers, H. Zhang, J. Wang, and M. Jiang, "Passively mode-locked Yb:LuVO₄ oscillator," *Opt. Express* **14**(24), 11668–11671 (2006).
7. V. E. Kisel, N. A. Tolstik, A. E. Troshin, N. V. Kuleshov, V. N. Matrosov, T. A. Matrosova, M. I. Kupchenko, F. Brunner, R. Paschotta, F. Morier-Genoud, and U. Keller, "Spectroscopy and femtosecond laser performance of Yb³⁺:Gd_{0.64}Y_{0.36}VO₄ crystal," *Appl. Phys. B* **85**(4), 581–584 (2006).
8. J. Liu, W. Han, H. Zhang, X. Mateos, and V. Petrov, "Comparative study of high-power continuous-wave laser performance of Yb-doped vanadate crystals," *IEEE J. Quantum Electron.* **45**(7), 807–815 (2009).

9. A. A. Belik, V. A. Morozov, R. N. Kotov, S. S. Khasanov, and B. I. Lazoryak, "Crystal structures of double vanadates $\text{Ca}_9\text{R}(\text{VO}_4)_7$: I. R= La, Pr, and Eu," *Crystallogr. Rep.* **42**(5), 751–757 (2000).
10. M. V. Dobrotvorskaya, Yu. N. Gorobets, M. B. Kosmyna, P. V. Mateichenko, B. P. Nazarenko, V. M. Puzikov, and A. N. Shekhovtsov, "Growth and characterization of $\text{Ca}_9\text{Ln}(\text{VO}_4)_7$ crystals ($\text{Ln} = \text{Y, La, or Gd}$)," *Crystallogr. Rep.* **57**(7), 959–961 (2012).
11. P. A. Loiko, A. S. Yasukevich, A. E. Gulevich, M. P. Demesh, M. B. Kosmyna, B. P. Nazarenko, V. M. Puzikov, A. N. Shekhovtsov, A. A. Kornienko, E. B. Dunina, N. V. Kuleshov, and K. V. Yumashev, "Growth, spectroscopic and thermal properties of Nd-doped disordered $\text{Ca}_9\text{La}(\text{VO}_4)_7$ and $\text{Ca}_{10}(\text{Li/K})(\text{VO}_4)_7$ laser crystals," *J. Lumin.* **137**, 252–258 (2013).
12. Z. Lin, G. Wang, and L. Zhang, "Growth of a new nonlinear optical crystal $\text{YCa}_9(\text{VO}_4)_7$," *J. Cryst. Growth* **304**(1), 233–235 (2007).
13. L. Li, G. Wang, Y. Huang, L. Zhang, Z. Lin, and G. Wang, "Crystal growth and spectral properties of $\text{Nd}^{3+}:\text{Ca}_9\text{Gd}(\text{VO}_4)_7$ crystal," *J. Cryst. Growth* **314**(1), 331–335 (2011).
14. P. N. Hu and G. F. Wang, "Growth and spectral properties of $\text{Er}^{3+}:\text{Ca}_9\text{La}(\text{VO}_4)_7$ crystal," *Mater. Res. Innov.* **15**(1), 75–77 (2011).
15. F. F. Yuan, W. Zhao, Y. S. Huang, L. Z. Zhang, S. J. Sun, Z. B. Lin, and G. F. Wang, "Growth and optical properties of a new promising laser material $\text{Er}^{3+}/\text{Yb}^{3+}:\text{Ca}_9\text{Y}(\text{VO}_4)_7$," *Opt. Commun.* **328**, 62–66 (2014).
16. L. Huang, N. Zhuang, G. Zhang, J. Chen, C. Huang, B. Zhao, Y. Wei, X. Hu, and M. Wei, "Accurate measurement of refractive indices of $\text{Ca}_9\text{La}(\text{VO}_4)_7$ crystal," *Opt. Mater.* **31**(2), 372–374 (2008).
17. R. Gopal and C. Calvo, "The structure of $\text{Ca}_3(\text{VO}_4)_2$," *Z. für Kristallographie-Crystalline Materials* **137**(1–6), 67–85 (1973).
18. L. Liu, R. Xie, N. Hirotsaki, Yu. Li, T. Takeda, C. Zhang, J. Li, and X. Sun, "Crystal structure and photoluminescence properties of red-emitting $\text{Ca}_9\text{La}_{1-x}(\text{VO}_4)_7:x\text{Eu}^{3+}$ phosphors for white light-emitting diodes," *J. Am. Ceram. Soc.* **93**(12), 4081–4086 (2010).
19. A. Grzechnik, "High-temperature transformations in calcium orthovanadate studied with Raman scattering," *Chem. Mater.* **10**(4), 1034–1040 (1998).
20. M. B. Kosmyna, B. P. Nazarenko, V. M. Puzikov, A. N. Shekhovtsov, W. Paszkowicz, A. Behrooz, P. Romanowski, A. S. Yasukevich, N. V. Kuleshov, M. P. Demesh, W. Wierzchowski, K. Wieteska, and C. Paulmann, " $\text{Ca}_{10}\text{Li}(\text{VO}_4)_7:\text{Nd}^{3+}$, a promising laser material: growth, structure and spectral characteristics of a Czochralski-grown single crystal," *J. Cryst. Growth* **445**, 101–107 (2016).
21. P. G. Zverev, A. Ya. Karasik, T. T. Basiev, L. I. Ivleva, and V. V. Osiko, "Stimulated Raman scattering of picosecond pulses in SrMoO_4 and $\text{Ca}_3(\text{VO}_4)_2$ crystals," *Quantum Electron.* **33**(4), 331–334 (2003).
22. P. Loiko, X. Mateos, S. Y. Choi, F. Rotermund, J. M. Serres, M. Aguiló, F. Díaz, K. Yumashev, U. Griebner, and V. Petrov, "Vibronic thulium laser at 2131 nm Q-switched by single-walled carbon nanotubes," *J. Opt. Soc. Am. B* **33**(11), D19–D27 (2016).
23. B. R. Judd, "Optical absorption intensities of rare-earth ions," *Phys. Rev.* **127**(3), 750–761 (1962).
24. G. S. Ofelt, "Intensities of crystal spectra of rare-earth ions," *J. Chem. Phys.* **37**(3), 511–520 (1962).
25. B. M. Walsh, N. P. Barnes, and B. Di Bartolo, "Branching ratios, cross sections, and radiative lifetimes of rare earth ions in solids: Application to Tm^{3+} and Ho^{3+} ions in LiYF_4 ," *J. Appl. Phys.* **83**(5), 2772–2787 (1998).
26. C. M. Dodson and R. Zia, "Magnetic dipole and electric quadrupole transitions in the trivalent lanthanide series: Calculated emission rates and oscillator strengths," *Phys. Rev. B* **86**(12), 125102 (2012).
27. A. S. Yasukevich, V. G. Shcherbitskii, V. E. Kisel, A. V. Mandrik, and N. V. Kuleshov, "Integral method of reciprocity in the spectroscopy of laser crystals with impurity centers," *J. Appl. Spectrosc.* **71**(2), 202–208 (2004).
28. R. Lisiecki, P. Solarz, G. Dominiak-Dzik, W. Ryba-Romanowski, M. Sobczyk, P. Černý, J. Šulc, H. Jelínková, Y. Urata, and M. Higuchi, "Comparative optical study of thulium-doped YVO_4 , GdVO_4 , and LuVO_4 single crystals," *Phys. Rev. B* **74**(3), 035103 (2006).
29. J. M. Serres, X. Mateos, P. Loiko, K. Yumashev, N. Kuleshov, V. Petrov, U. Griebner, M. Aguiló, and F. Díaz, "Diode-pumped microchip $\text{Tm}:\text{KLu}(\text{WO}_4)_2$ laser with more than 3 W of output power," *Opt. Lett.* **39**(14), 4247–4250 (2014).

1. Introduction

Vanadate crystals represent an important class of host materials for doping with laser-active trivalent lanthanide ions, $\text{Ln}^{3+} = \text{Yb}^{3+}, \text{Nd}^{3+}, \text{Tm}^{3+}, \text{Ho}^{3+}$, etc. A well-known example is the family of the tetragonal zircon-type REVO_4 crystals where RE stands for Y, Gd or Lu [1]. In recent years, REVO_4 crystals doped with Yb^{3+} and Tm^{3+} ions were used in efficient and broadly tunable continuous-wave (CW), Q-switched and mode-locked (ML) lasers operating at ~ 1 and $2 \mu\text{m}$ [2–6]. Additional broadening of the spectral bands of the Ln^{3+} ions enables shorter pulses to be generated by ML lasers. For this reason "mixed" $\text{Y}_x\text{Gd}_y\text{Lu}_z\text{VO}_4$ crystals doped with Yb^{3+} were also studied [7,8].

There is a different crystal family of trigonal calcium vanadates, with the chemical formula $\text{Ca}_9\text{RE}^{3+}(\text{VO}_4)_7$ where RE = La, Y, Gd, Lu or Bi [9–11]. The first studies of these non-centrosymmetric (point group: 3m) crystals were focused on their nonlinear properties for second-harmonic generation (SHG) [12]. In recent years, they are being studied as laser

host materials for Ln^{3+} dopants [13–15]. A partially disordered structure of the $Ca_9RE(VO_4)_7$ crystals promotes broadening of the spectral bands of the active ions [11] which is of interest for tunable operation and the generation of ultrashort pulses. The $Ca_9RE(VO_4)_7$ crystals are uniaxial [16] and they can provide naturally polarized laser output. These materials possess relatively low anisotropy of the thermal expansion ($\alpha_a/\alpha_c \sim 1.5\text{--}2$) and they are expected to feature “athermal” thermo-optic behavior [11] which may overcome the disadvantage of its low thermal conductivity (~ 1 W/mK). The $Ca_9RE(VO_4)_7$ compounds melt congruently and large-volume crystals can be grown by the Czochralski method [10]. Spectroscopic properties of some of the Ln^{3+} ions in the $Ca_9RE(VO_4)_7$ -type crystals have been studied [11,13–15].

Thulium (Tm^{3+}) ions are attractive for laser operation around $2\ \mu\text{m}$. Such an emission is eye-safe and absorbed in water in the atmosphere and bio-tissues. Tm lasers are thus used in range-finding, remote sensing and medicine. To date, the Tm^{3+} ions have been doped into numerous oxide and fluoride host materials, e.g. $Y_3Al_5O_{12}$, Lu_2O_3 , YVO_4 , $KLu(WO_4)_2$, $YAlO_3$, $LiYF_4$, *etc.*, and efficient and wavelength-tunable laser operation in the $1.8\text{--}2.1\ \mu\text{m}$ spectral range (depending on the host) has been achieved. In the present work, we report on the crystal growth and a detailed spectroscopic study of a novel trigonal crystal, $Tm:Ca_9La(VO_4)_7$. Its properties designate $Tm:Ca_9La(VO_4)_7$ for applications in broadband tunable and ultrashort pulse lasers at $\sim 2\ \mu\text{m}$.

2. Crystal growth and structure

The $Tm:Ca_9La(VO_4)_7$ crystal was grown by the Czochralski method. The raw materials used for crystal growth were synthesized by traditional high temperature solid-state reaction method. The chemicals $CaCO_3$, V_2O_5 (analytical reagent grade), and La_2O_3 , Tm_2O_3 with 4N purity, were weighed according to the $9CaCO_3 + 0.47La_2O_3 + 0.03Tm_2O_3 + 3.5V_2O_5 \rightarrow Ca_9La_{0.94}Tm_{0.06}(VO_4)_7 + 9CO_2\uparrow$ reaction. The mixtures were ground in an agate mortar for blending well, and extruded to form pellets. Then, these pellets were placed into an alumina crucible and sintered in a muffle furnace at $1000\ ^\circ\text{C}$ for 48 h. These processes were repeated, and the sintering temperature was raised to $1200\ ^\circ\text{C}$ to ensure complete reaction. The formation of the trigonal $Ca_9La(VO_4)_7$ phase was confirmed by X-ray power diffraction (XRD).

The crystal was grown in an iridium crucible with dimensions of $\text{Ø}27 \times 26\ \text{mm}^3$, in a 25 kHz mid-frequency induction furnace (DJL-400) in a N_2 atmosphere, with a pulling rate of 1–1.5 mm/h and a rotation rate of 8–12 rpm. A $[001]$ oriented $Ca_9La(VO_4)_7$ crystal was used as a seed. When the growth process ended, the grown crystal was pulled slowly out of the melt, and cooled to room temperature at a rate of $15\text{--}30\ ^\circ\text{C}/\text{h}$. Large-volume boules of $Tm:Ca_9La(VO_4)_7$ 30 mm in length and 25 mm in diameter were obtained, Fig. 1(a). The coloration of the as-grown crystals ranged from dark-yellow to green. This is an indication of the presence of color centers which is typical for disordered Ca vanadates grown in anoxic conditions [13]. The formation of color centers is due to the reduction of the V^{5+} ions to V^{4+} and V^{3+} and the appearance of oxygen vacancies. In order to eliminate these effects which will be detrimental for potential laser applications, and to reduce the thermal stress, the grown crystal was annealed at $1200\ ^\circ\text{C}$ for 24 h in air. This improved the transparency of the crystal and its coloration changed to yellowish, Fig. 1(b).

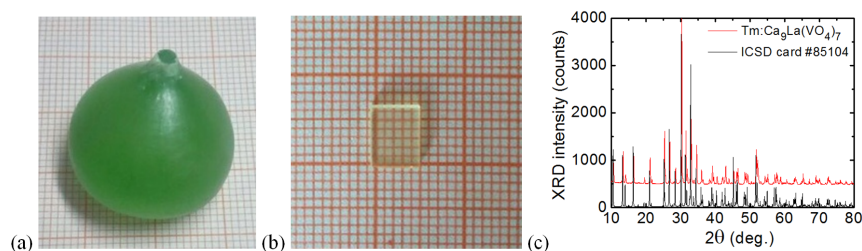


Fig. 1. (a) As-grown $Tm:Ca_9La(VO_4)_7$ boule; (b) annealed in air and polished 1 mm-thick plate cut from this boule; XRD pattern of the powdered $Tm:Ca_9La(VO_4)_7$ crystal.

The XRD data for the grown crystal were collected at room temperature in the $2\theta = 10\text{--}80^\circ$ range with a step of 0.02° and a scan speed of $0.13^\circ/\text{min}$, using a Desktop X-ray diffractometer (Rigaku, Miniflex 600) equipped with Cu $K\alpha$ radiation. The XRD pattern of the powdered as-grown crystal is shown in Fig. 1(c). The diffraction peaks match perfectly the standard pattern of undoped $\text{Ca}_9\text{La}(\text{VO}_4)_7$ (ICSD card #85104). The concentration of the Tm^{3+} ions in the grown crystal N_{Tm} was measured by an Inductively Coupled Plasma OES spectrometer (HORIBA Jobin Yvon, Ultima 2), resulting in a value of $N_{\text{Tm}} = 0.88 \times 10^{20}$ at/cm^3 or 5.72 at.%. Consequently, the segregation coefficient of Tm^{3+} ions is $K_{\text{Tm}} = 0.95$ which indicates that they can easily substitute the “passive” La^{3+} ions.

The $\text{Ca}_9\text{RE}(\text{VO}_4)_7$ vanadates are isostructural to the double calcium vanadate, $\text{Ca}_3(\text{VO}_4)_2$ or $\text{Ca}_{10.5}(\text{VO}_4)_7$ (sp.gr. $R3c$), which is considered as a parent compound [17]. The trigonal whitlockite-like structure of $\text{Ca}_9\text{La}(\text{VO}_4)_7$ is formed as a result of a distortion of the $\text{Ca}_3(\text{VO}_4)_2$ one when the La^{3+} ions partially occupy the cationic positions of the Ca^{2+} ions [9,18], see Fig. 2(a). Since the difference of the ionic radii of the La^{3+} and Ca^{2+} ions is relatively small, the $\text{Ca}_9\text{La}(\text{VO}_4)_7$ structure is isomorphic to that of $\text{Ca}_3(\text{VO}_4)_2$ while disordering of the cationic positions occurs. The $\text{Ca}_9\text{RE}(\text{VO}_4)_7$ structure has four cationic sites with different occupancy numbers [9,17,18]: three low-symmetry sites (point group C_1): $Me(1)$, $Me(2)$ and $Me(3)$ with coordination numbers 9, 8, and 7, respectively, and a 6-fold coordinated (octahedral) cationic site $Me(4)$, as shown in Fig. 2(b). For an undoped $\text{Ca}_9\text{La}(\text{VO}_4)_7$, the Ca^{2+} and La^{3+} ions occupy randomly the same $Me(1) - Me(4)$ sites in an overall proportion of 9:1 (the occupancy number for the $Me(4)$ site is close to 1 for the Ca^{2+} ions). In the Ln^{3+} -doped $\text{Ca}_9\text{La}(\text{VO}_4)_7$ crystals, the Ln^{3+} and La^{3+} ions are randomly distributed over the $Me(1) - Me(3)$ cationic positions without inversion symmetry (together with the Ca^{2+} ions). For the $Me(1)$, $Me(2)$ and $Me(3)$ sites, the average $\text{Ln}^{3+}/\text{La}^{3+}/\text{Ca}^{2+}-\text{O}^{2-}$ distances are ~ 2.4 , 2.5 , and 2.6 Å, respectively. The shortest $\text{Ln}^{3+} - \text{Ln}^{3+}$ distance is ~ 3.6 Å. Based on the XRD analysis, we determined the lattice constants for $\text{Tm}:\text{Ca}_9\text{La}(\text{VO}_4)_7$ as $a = b = 10.846$ Å, $c = 37.901$ Å ($V = 3861.2$ Å³ and $Z = 6$), slightly shorter than for the undoped crystal ($a = 10.8987$ Å, $c = 38.1470$ Å) [9]. This is attributed to the difference in ionic radii of the dopant Tm^{3+} and the substituted La^{3+} ions (0.994 Å and 1.160 Å, respectively, e.g., for the 8-fold O^{2-} -coordination). The calculated density of $\text{Tm}:\text{Ca}_9\text{La}(\text{VO}_4)_7$ is $\rho = 3.746$ g/cm^3 .

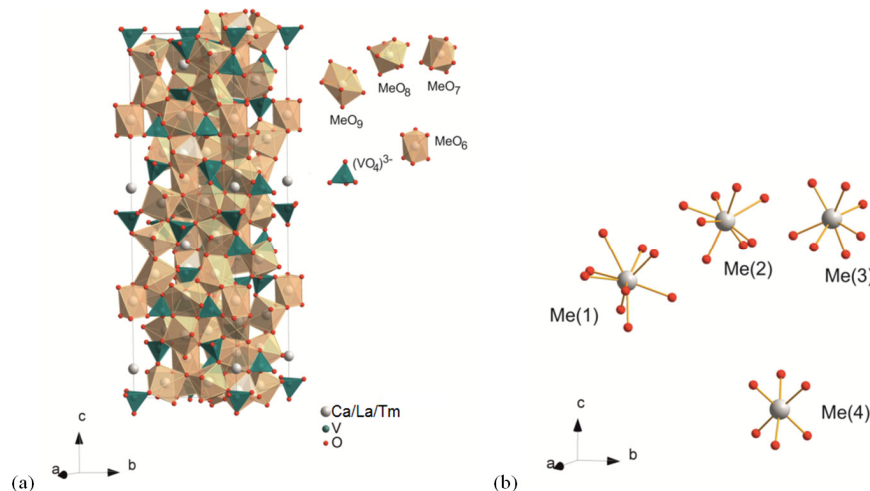


Fig. 2. (a) Fragment of the structure of the $\text{Tm}:\text{Ca}_9\text{La}(\text{VO}_4)_7$ crystal within one unit-cell; (b) oxygen coordination of metal ions in the four possible sites.

The vibrational properties of the $\text{Tm}:\text{Ca}_9\text{La}(\text{VO}_4)_7$ crystal were studied with polarized Raman spectroscopy. The Raman spectra recorded for the $x'(xy)y'$ geometries with $x, y = \pi$ or σ and $x' = y' = a$ are shown in Fig. 3. The excitation wavelength was 514 nm. Here we use standard notations where x' and y' represent the direction of propagation of the excitation and

scattered light, and x and y stand for the polarization of the excitation and scattered light, respectively. The Raman bands are observed in two separate ranges: 200–470 cm^{-1} and 740–930 cm^{-1} which are similar to the Raman spectrum of the parent compound, $\text{Ca}_3(\text{VO}_4)_2$ [19]. The Raman bands in the low-frequency range are assigned to the O–V–O bending modes and to the Ca^{2+} cation displacements. The high-frequency Raman bands are attributed to the V–O stretching modes and possible vibrations of the V–O–...La/Tm chain [20]. The strongest Raman signal is observed for the $a(\pi\sigma)a$ geometry. The most intense band is at 867 cm^{-1} with a full width at half maximum (FWHM) of 26.6 cm^{-1} . This stretching mode is assigned as $\nu(A_1)$. The broadening of the Raman bands is due to the disordered nature of the material. The parent compound, $\text{Ca}_3(\text{VO}_4)_2$, has been used for stimulated Raman scattering (SRS) of picosecond pulses [21]. The broad and intense Raman bands of $\text{Tm}:\text{Ca}_9\text{La}(\text{VO}_4)_7$ make it also interesting for self-SRS. In addition, the low-energy bands around $\sim 350 \text{ cm}^{-1}$ can provide vibronic Tm laser operation as further extension of the tuning capability [22].

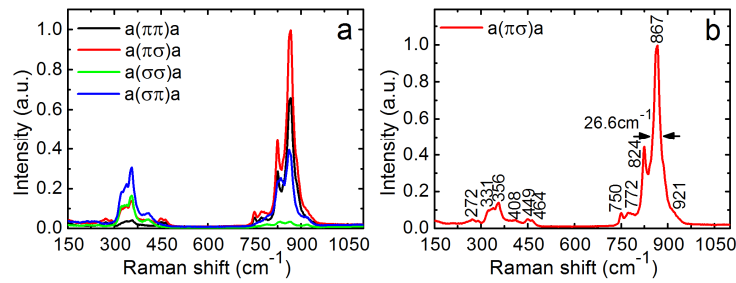


Fig. 3. Raman spectra for an a -cut $\text{Tm}:\text{Ca}_9\text{La}(\text{VO}_4)_7$ crystal excited at 514 nm: (a) polarization dependence in the $a(xy)a$ geometry; (b) details of the spectrum for the $a(\pi\sigma)a$ geometry.

3. Spectroscopic characterization

The $\text{Ca}_9\text{La}(\text{VO}_4)_7$ crystal is an optically uniaxial birefringent crystal (point group $R3c$). Its optical axis is parallel to the c -axis. At $\sim 1.85 \mu\text{m}$, the two principal refractive indices of $\text{Ca}_9\text{La}(\text{VO}_4)_7$ are $n_o = 1.841$ and $n_e = 1.808$ [16] (positive uniaxial crystal). The spectral properties are described for the two principal light polarizations, $E \parallel c$ (π) and $E \perp c$ (σ).

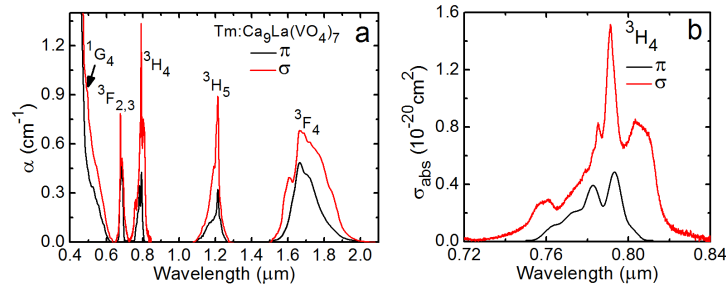


Fig. 4. (a) Absorption spectrum of the 5.72 at.% $\text{Tm}:\text{Ca}_9\text{La}(\text{VO}_4)_7$ crystal; (b) absorption cross-sections σ_{abs} for the ${}^3\text{H}_6 \rightarrow {}^3\text{H}_4$ transition of the Tm^{3+} ion.

The absorption spectrum of the $\text{Tm}:\text{Ca}_9\text{La}(\text{VO}_4)_7$ crystal for the π - and σ -polarizations is shown in Fig. 4(a). It was measured at room temperature. For the absorption band related to the ${}^3\text{H}_6 \rightarrow {}^3\text{H}_4$ transition of the Tm^{3+} ion which is suitable for pumping at around 800 nm with commercial AlGaAs laser diodes, the maximum absorption cross-section is $1.5 \times 10^{-20} \text{ cm}^2$ at 791.3 nm for σ -polarization, determined as $\sigma_{\text{abs}} = \alpha/N_{\text{Tm}}$ where α is the absorption coefficient. The FWHM of the local peak is 8.2 nm. For π -polarization, σ_{abs} is ~ 3 times lower. The UV absorption edge for the $\text{Tm}:\text{Ca}_9\text{La}(\text{VO}_4)_7$ crystal is at $\lambda_g = 0.44 \mu\text{m}$ ($E_g = 2.82 \text{ eV}$).

The absorption oscillator strengths for the Tm^{3+} ion in $\text{Ca}_9\text{La}(\text{VO}_4)_7$ were determined from the measured absorption spectrum:

$$f_{\text{exp}}(JJ') = \frac{m_e c^2}{\pi e^2 N_{\text{Tm}} \langle \lambda \rangle^2} \Gamma(JJ'), \quad (1)$$

where m_e and e are the electron mass and charge, respectively, c is the speed of light, $\Gamma(JJ')$ is the integrated absorption coefficient within the absorption band and $\langle \lambda \rangle$ is the “center of gravity” of the absorption band. The experimental absorption oscillator strengths were averaged over the principal light polarizations, $1/3 \times (2f_\sigma + f_\pi)$. The results are shown in Table 1.

The values of f_{exp} were used to determine the intensity parameters, Ω_2 , Ω_4 and Ω_6 , within the standard Judd-Ofelt (J-O) theory [23,24]. $\Omega_2 = 4.682$, $\Omega_4 = 0.659$ and $\Omega_6 = 0.475$ [10^{-20} cm^2]. Using these parameters, the absorption oscillator strengths were also calculated:

$$f_{\text{calc}}(JJ') = \frac{8}{3h(2J'+1)\langle \lambda \rangle} \frac{(n^2 + 2)^2}{9n} S_{\text{calc}}(JJ') + f_{\text{MD}}(JJ'), \quad (2a)$$

$$S_{\text{calc}}(JJ') = \sum_{k=2,4,6} U^{(k)} \Omega_k, \text{ where } U^{(k)} = \langle (4f^n)SLJ || U^k || (4f^n)S'L'J' \rangle^2. \quad (2b)$$

Here, S_{calc} are the line strengths, h is the Planck constant, n is the refractive index of the crystal and $U^{(k)}$ are the squared reduced matrix elements [25]. The J-O theory describes electric-dipole (ED) transitions. The contribution of magnetic-dipole (MD) transitions with $J-J' = 0, \pm 1, f_{\text{MD}}$, was taken from the literature [26].

Table 1. Experimental and Calculated Absorption Oscillator Strengths for the $\text{Tm}:\text{Ca}_9\text{La}(\text{VO}_4)_7$ Crystal

Transition	$\langle \lambda \rangle$, nm	$\langle E \rangle$, cm^{-1}	Γ , cm^{-1}nm	$f_{\text{exp}} \times 10^6$	$f_{\text{calc}} \times 10^6$
${}^3\text{H}_6 \rightarrow {}^3\text{F}_4$	1667	5998	118.29	3.25	3.24 ^{ED}
${}^3\text{H}_6 \rightarrow {}^3\text{H}_5$	1214	8237	31.76	2.56	1.52 ^{ED} + 0.57 ^{MD}
${}^3\text{H}_6 \rightarrow {}^3\text{H}_4$	792.0	12626	27.80	3.71	3.59 ^{ED}
${}^3\text{H}_6 \rightarrow {}^3\text{F}_3$	686.0	14577	10.96	1.96	1.76 ^{ED}
${}^3\text{H}_6 \rightarrow {}^1\text{G}_4$	473.0	21141	3.83	1.41	1.37 ^{ED}

$\langle \lambda \rangle$ - “center of gravity” of the absorption band, $\langle E \rangle$ - corresponding estimated energy of the multiplet barycenter, Γ - integrated absorption coefficient, f_{exp} and f_{calc} - experimental and calculated absorption oscillator strengths, respectively, ED and MD stand for the electric-dipole and magnetic-dipole contributions, respectively.

The probabilities of spontaneous radiative transitions were calculated from the corresponding line strengths which, in turn, are derived from the J-O parameters Ω_k and squared reduced matrix elements $U^{(k)}$, see Eq. (2)b):

$$A_{\text{calc}}(JJ') = \frac{64\pi^4 e^2}{3h(2J'+1)\langle \lambda \rangle^3} n \left(\frac{n^2 + 2}{3} \right)^2 S_{\text{ED}}^{\text{calc}}(JJ') + A_{\text{MD}}(JJ') \quad (3)$$

The MD contributions A_{MD} were taken from [26]. On the basis of the probability of spontaneous transitions for the separate emission channels $J \rightarrow J'$, we calculated the total probability, A_{tot} , the corresponding radiative lifetime of the excited-state, τ_{rad} , and the luminescence branching ratios for the emission channels, $B(JJ')$:

$$A_{\text{tot}} = \sum_{J'} A_{\text{calc}}(JJ') \text{ and } \tau_{\text{rad}} = \frac{1}{A_{\text{tot}}}, \quad (4a)$$

$$B(JJ') = \frac{A_{\text{calc}}(JJ')}{\sum_{J'} A_{\text{calc}}(JJ')} \quad (4b)$$

The results are summarized in Table 2. In particular, the radiative lifetime of the lowest excited-state, $\tau_{\text{rad}}(^3F_4) = 2.02$ ms.

The photoluminescence (PL) spectra for the Tm^{3+} -doped $\text{Ca}_9\text{La}(\text{VO}_4)_7$ crystal were measured with unpolarized light under excitation to the 3H_4 state at ~ 0.79 μm using a tunable Ti:Sapphire laser, see Fig. 5. The PL from the excited level is observed at 0.78-0.82 μm ($^3H_4 \rightarrow ^3H_6$ transition) and at 1.4-1.55 μm ($^3H_4 \rightarrow ^3F_4$ transition). A broad band spanning from 1.6 to 2.05 μm is due to the $^3F_4 \rightarrow ^3H_6$ transition from the upper laser level. In addition, several emissions in the visible (centered at ~ 0.48 μm and at ~ 0.7 μm) and near-IR (at ~ 1.07 μm) are detected which are related to the radiative transitions from the higher-lying 1G_4 and $^3F_{2,3}$ states of Tm^{3+} . These states are populated by the excited-state absorption (ESA) process $^3H_5 \rightarrow ^1G_4$ (for the 1G_4 state) and the same ESA with a subsequent non-radiative relaxation (for the $^3F_{2,3}$ states). A weak PL of Er^{3+} impurity is also observed at ~ 0.52 , 0.54 and 1 μm . The presence of Er^{3+} in the studied crystal may be due to impurities in the Tm_2O_3 reagent. Then, the Er^{3+} ions are excited by an energy-transfer process $\text{Tm}^{3+}(^3H_4) \rightarrow \text{Er}^{3+}(^4I_{9/2})$ which is very probable because these two states are resonant in energy. The green emission from Er^{3+} originates from the $^4S_{3/2} + ^2H_{11/2} \rightarrow ^4I_{15/2}$ transition and the near-IR emission from the $^4I_{11/2} \rightarrow ^4I_{15/2}$ one. As a result, visible PL from the $\text{Tm}:\text{Ca}_9\text{La}(\text{VO}_4)_7$ crystal has a green-bluish color.

Table 2. Calculated Emission Probabilities for the Tm^{3+} Ion in $\text{Ca}_9\text{La}(\text{VO}_4)_7$ Crystal

Excited state	Final state	$\langle \lambda \rangle$, nm	$A_{JJ'}$, s ⁻¹	$B_{JJ'}$, %	A_{tot} , s ⁻¹	τ_{rad} , ms
3F_4	3H_6	1667	495.7 ^{ED}	100	495.7	2.02
3H_5	3F_4	4467	9.1 ^{ED} + 1.5 ^{MD}	1.8	590.2	1.69
	3H_6	1214	426.1 ^{ED} + 153.5 ^{MD}	98.2		
3H_4	3H_5	2279	22.4 ^{ED} + 17.3 ^{MD}	1.2	3190	0.31
	3F_4	1509	229.1 ^{ED} + 42.0 ^{MD}	8.5		
	3H_6	792.1	2879 ^{ED}	90.3		
$^3F_3 + ^3F_2$	3H_4	5121	3.4 ^{ED} + 0.2 ^{MD}	0.1	3457	0.29
	3H_5	1577	846.9 ^{ED}	24.5		
	3F_4	1166	102.9 ^{ED} + 108.1 ^{MD}	6.1		
	3H_6	686.0	2395 ^{ED}	69.3		
1G_4	3F_2	1641	16.2 ^{ED}	44.2	5877	0.17
	3F_3	1523	52.7 ^{ED} + 6.2 ^{MD}	0.3		
	3H_4	1174	478.7 ^{ED} + 61.8 ^{MD}	1.0		
	3H_5	774.9	1151 ^{ED} + 293.5 ^{MD}	9.2		
	3F_4	660.4	231.7 ^{ED} + 18.3 ^{MD}	24.6		
	3H_6	473.0	3567 ^{ED}	4.3		

$\langle \lambda \rangle$ - mean wavelength of the emission band, $A_{JJ'}$ - probability of radiative spontaneous transition, $B_{JJ'}$ - luminescence branching ratio, A_{tot} and τ_{rad} - total probability of radiative spontaneous transitions and radiative lifetime of the excited state, respectively; ED and MD stand for the electric-dipole and magnetic-dipole contributions, respectively.

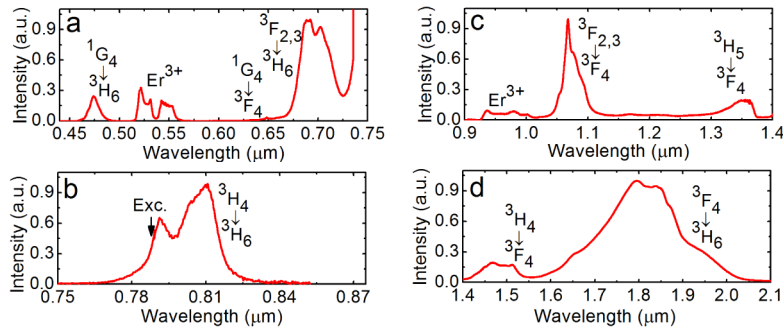


Fig. 5. PL spectra for Tm³⁺-doped Ca₉La(VO₄)₇ crystal (unpolarized light, excitation wavelength is 0.79 μm): (a) visible and (b-d) near-IR emissions.

The stimulated-emission (SE) cross-section, σ_{SE} , spectra corresponding to the ${}^3F_4 \rightarrow {}^3H_6$ transition of the Tm³⁺ ion in Ca₉La(VO₄)₇ were calculated using the modified reciprocity method [27]:

$$\sigma_{SE}^i(\lambda) = \frac{1}{8\pi n_i^2 \tau_{rad} c} \frac{3\sigma_{abs}^i(\lambda) \exp(-hc/(kT\lambda))}{\sum_{i=\pi,\sigma} \int \lambda^{-4} \sigma_{abs}^i(\lambda) \exp(-hc/(kT\lambda)) d\lambda} \quad (5)$$

Here, σ_{SE}^i and σ_{abs}^i ($i = \pi$ or σ) are the SE and absorption cross-sections for the i -th principal light polarization, respectively, τ_{rad} is the radiative lifetime of the emitting state (3F_4 state of Tm³⁺) determined with the J-O theory. The results on the SE cross-sections are shown in Fig. 6(a). The maximum value of σ_{SE} is $1.28 \times 10^{-20} \text{ cm}^2$ at 1854 nm for σ -polarization. This value is ~ 3 times larger than for π -polarized light, $0.38 \times 10^{-20} \text{ cm}^2$ at 1858 nm. The strong polarization-anisotropy of σ_{SE} was observed by direct measurement of the luminescence intensity for the two polarizations.

The results on the luminescence decay for the Tm:Ca₉La(VO₄)₇ crystal are presented in Fig. 6(b). By exciting the Tm³⁺ ions at 0.79 μm, we monitored the decay from the 3F_4 upper laser level (at 1.85 μm) and the 3H_4 pump state (at 0.8 μm). The sample was powdered and immersed in glycerin (10 wt.% of powder in the solution) in order to prevent the effect of reabsorption on the measured lifetime. The decay curves are clearly single-exponential. The determined lifetimes are $\tau_{exp}({}^3F_4) = 1.19 \text{ ms}$ and $\tau_{exp}({}^3H_4) = 122 \mu\text{s}$. The shortening of the experimental lifetime of the upper laser level with respect to the radiative lifetime, expressed by a quantum yield of luminescence of $\eta_q = \tau_{exp}/\tau_{rad} = 59\%$, is partially attributed to the non-radiative relaxation probably related to the color centers which are not completely eliminated even after crystal annealing, to the concentration quenching which is also rather strong in, cf. Tm:REVO₄ crystals [28], and to the excitation transfer to the Er³⁺ impurities.

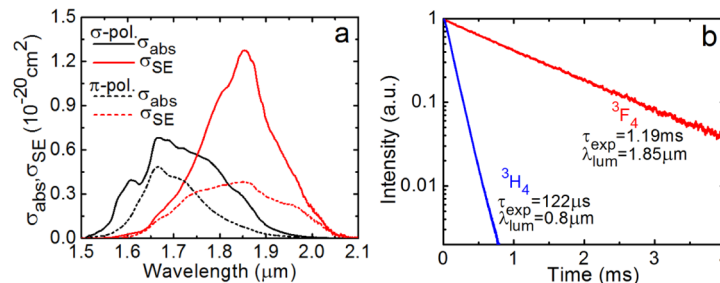


Fig. 6. (a) Absorption, σ_{abs} , and stimulated-emission, σ_{SE} , cross-sections for the ${}^3H_6 \leftrightarrow {}^3F_4$ transition of the Tm³⁺ ion in Ca₉La(VO₄)₇ crystal for the π - and σ -polarizations; (b) measured decay of luminescence from the 3F_4 upper laser level (at 1.85 μm) and the 3H_4 pump state (at 0.8 μm); the excitation wavelength is $\sim 0.79 \mu\text{m}$.

An important parameter for quasi-three-level laser materials, e.g. Tm^{3+} -doped ones, is the gain cross-section, $\sigma_g = \beta\sigma_{\text{SE}} - (1 - \beta)\sigma_{\text{abs}}$ where $\beta = N_2/N_{\text{Tm}}$ is the inversion ratio and N_2 is the population of the upper laser level, ${}^3\text{F}_4$. The results on σ_g for the $\text{Tm}:\text{Ca}_9\text{La}(\text{VO}_4)_7$ crystal are shown in Fig. 7.

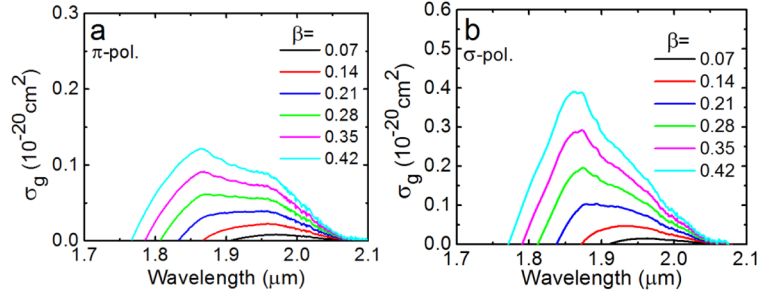


Fig. 7. Gain cross-sections, $\sigma_g = \beta\sigma_{\text{SE}} - (1 - \beta)\sigma_{\text{abs}}$, for the ${}^3\text{F}_4 \rightarrow {}^3\text{H}_6$ transition of the Tm^{3+} ion in $\text{Ca}_9\text{La}(\text{VO}_4)_7$ crystal for the π - (a) and σ - (b) polarizations; $\beta = N_2({}^3\text{F}_4)/N_{\text{Tm}}$ is the inversion ratio.

The gain cross-sections are much higher for σ -polarization as compared with π -polarization. The uniaxial crystals offer two principal orientations of the laser elements, denoted as a -cut and c -cut. For a laser based on an a -cut $\text{Tm}:\text{Ca}_9\text{La}(\text{VO}_4)_7$ crystal and containing no polarizing elements, we expect linearly (σ -) polarized laser output; and for a c -cut crystal, it will be unpolarized. For the σ -polarization at low $\beta < 0.05$, a broad gain spectrum spanning from 1.9 to 2.05 μm is observed. With an increase of β , a local peak is formed in the gain spectra shifting from $\sim 1.93 \mu\text{m}$ ($\beta \sim 0.1$) to $1.86 \mu\text{m}$ ($\beta > 0.1$). In contrast, the π -polarization impresses by a broad gain smoothness up to high inversion levels of $\beta \sim 0.3$. In general, the gain spectra for $\text{Tm}:\text{Ca}_9\text{La}(\text{VO}_4)_7$ are broad and structureless. Thus, one can expect broad tuning of the laser emission from ~ 1.8 to $2.05 \mu\text{m}$.

From the point of view of the spectroscopic properties, both a - and c -cut $\text{Tm}:\text{Ca}_9\text{La}(\text{VO}_4)_7$ crystals are attractive for laser operation as they offer access to the high-gain σ -polarization. Under laser-pumping, the same pump polarization is preferable for high pump efficiency. The thermo-optic coefficients are negative for the $\text{Ca}_9\text{La}(\text{VO}_4)_7$ crystal: $dn_o/dT = -13.2$ and $dn_e/dT = -12.4 \times 10^{-6} \text{ K}^{-1}$ at $\sim 1.85 \mu\text{m}$ [11]. However, for an a -cut crystal, one can expect a positive thermal lens due to an “athermal” compensation of the negative contribution of dn_e/dT and the positive contribution of the large thermal expansion along the a -axis, $\alpha_a = 17.5 \times 10^{-6} \text{ K}^{-1}$ [11]. This may potentially enable microchip laser operation where the positive thermal lens plays a key role in the mode stabilization in a plano-plano laser cavity [29]. For a c -cut crystal, the thermal lens is expected to be negative due to much weaker thermal expansion along this direction, as $\alpha_a/\alpha_c \sim 1.9$. Thus, one can conclude that a -cut $\text{Tm}:\text{Ca}_9\text{La}(\text{VO}_4)_7$ crystals are more attractive for laser operation.

4. Conclusion

We report on the Czochralski growth and detailed spectroscopic characterization (including study of absorption, emission and Raman spectra, luminescence decay, transition cross-sections and Judd-Ofelt modeling) of a novel trigonal crystal, $\text{Tm}^{3+}:\text{Ca}_9\text{La}(\text{VO}_4)_7$. This work represents the first description of the optical properties of the Tm^{3+} ion in calcium vanadate single crystals. The disordered multi-site structure of $\text{Ca}_9\text{La}(\text{VO}_4)_7$ results in broad and structureless absorption and emission bands of the Tm^{3+} ions while preserving the polarization anisotropy of the optical properties. According to the analysis of the spectroscopy and thermo-optics of $\text{Tm}:\text{Ca}_9\text{La}(\text{VO}_4)_7$, the preferred orientation for laser operation is a -cut (σ -polarization). The maximum SE cross-section corresponding to the ${}^3\text{F}_4 \rightarrow {}^3\text{H}_6$ transition is $1.28 \times 10^{-20} \text{ cm}^2$ at 1854 nm for the σ -polarization. According to the gain spectra in both polarizations, broadband tunable laser emission at 1.8 - $2.05 \mu\text{m}$ and ultrashort

pulse generation may be achieved. $\text{Tm}:\text{Ca}_9\text{La}(\text{VO}_4)_7$ possesses relatively long storage time in the upper laser level, ~ 1.2 ms for 5.72 at.% Tm doping, which is beneficial for passive Q-switching. Future work on $\text{Tm}:\text{Ca}_9\text{La}(\text{VO}_4)_7$ should be focused on the reduction of non-radiative quenching via proper annealing and purification of the raw materials which may provide higher luminescence quantum yield. In addition, $\text{Tm}:\text{Ca}_9\text{La}(\text{VO}_4)_7$ crystals are promising Raman and self-Raman frequency shifters.

Funding

The National Natural Science Foundation of China (11404332, 61575199, 21427801); Key Project of Science and Technology of Fujian Province (2016H0045); the Strategic Priority Research Program of the Chinese Academy of Sciences (XDB20000000); the National Key Research and Development Program of China (2016YFB0701002); the China Scholarship Council (CSC, 201504910418 and 201504910629); the Instrument project of Chinese Academy of Sciences (YZ201414); Spanish Government (MAT2016-75716-C2-1-R, MAT2013-47395-C4-4-R, TEC 2014-55948-R); Generalitat de Catalunya (2014SGR1358); Government of the Russian Federation (Grant 074-U01); ICREA (2010ICREA-02); European Union's Horizon 2020 (654148); Marie Skłodowska-Curie (657630).

Acknowledgments

P. Loiko acknowledges financial support from the Government of the Russian Federation (Grant 074-U01) through ITMO Post-Doctoral Fellowship scheme. F.D. acknowledges additional support through the ICREA academia award 2010ICREA-02 for excellence in research. This work has received funding from the European Union's Horizon 2020 research and innovation programme under grant agreement No 654148 Laserlab-Europe and under the Marie Skłodowska-Curie grant agreement No 657630.